Available online at www.sciencedirect.com
ScienceDirect
Journal of Catalysis 255 (2008) 104–113
JOURNAL OF CATALYSIS
www.elsevier.com/locate/jcat

Fe-based Fischer–Tropsch synthesis catalysts containing carbide-forming transition metal promoters

Nattaporn Lohitharn, James G. Goodwin Jr. *, Edgar Lotero

Department of Chemical and Biomolecular Engineering, Clemson University, Clemson, SC 29634, USA

Received 15 November 2007; revised 9 January 2008; accepted 24 January 2008

Abstract

Surprisingly, although the impacts of promoters such as K and Cu on the activity of Fe catalysts have been studied extensively, the effects of many other potential promoters for Fe catalysts similar to the commercial Ruhrchemie catalyst have not been significantly investigated or compared directly in a comprehensive study reported in the literature. In this study, the impact of adding various different transition metals (Cr, Mn, Mo, Ta, V, W, and Zr) on the catalytic properties of precipitated bulk Fe-based catalysts was investigated using the same preparation method and reaction conditions. All of the Fe catalysts prepared in this study exhibited high BET surface areas with excellent metal distributions. The addition of the third metal in addition of Fe and Cu (all except W) increased the activity of the Fe catalyst for CO hydrogenation and for the water–gas shift (WGS) reaction, with Cr-, Mn- and Zr-promoted Fe-based catalysts exhibiting the highest catalytic activities. However, hydrocarbon selectivity was not affected by the presence or type of added third metal. The enhanced activity of the Fe catalyst by third metal promotion (with the exception of Mn and Zr) appears to have been primarily due to a higher degree of Fe dispersion on the surface of catalyst whereas the higher activities observed for Mn- and Zr-promoted Fe catalysts were especially due to higher TOF_{chem} values based on CO chemisorption.

Keywords: Fischer–Tropsch synthesis (FTS); CO hydrogenation; Cr promotion; Mn promotion; Mo promotion; Ta promotion; V promotion; W promotion; Zr promotion; Water–gas shift (WGS); Fe-based FTS catalysts

1. Introduction

Gasification followed by Fischer–Tropsch synthesis (FTS) is an established technological route for upgrading natural gas, coal, and biomass to liquid fuels and other chemical products. Fe and Co catalysts are currently used in industrial practice. Although Fe catalysts are not as active as Co-based catalysts, they show high water–gas shift (WGS) activity, which makes Fe catalysts more suitable for the conversion of low H_2/CO ratio syngas derived from coal or biomass [1–3]. Commercial-grade Fe catalysts for FTS typically consist initially of bulk Fe oxide promoted with Cu (a reduction promoter), K (a chemical promoter), and SiO_2 (a structural promoter). Adding Cu to Fe catalysts facilitates reduction of Fe_2O_3 to Fe_3O_4 or metallic Fe [1,2,4–6]. The addition of SiO_2 is used to increase the surface area of the catalyst and to improve its attrition resistance, which is needed for FTS in a slurry phase reactor [5,7]. Longer-chain hydrocarbon products and better olefin selectivities are promoted by the addition of K [2,3].

Numerous studies have shown that the addition of transition metals can result in an enhancement of the activity of Fe-based FTS catalysts. For instance, Mn-promoted Fe catalysts (FeMn where Mn $<15\%$) demonstrated higher light olefin (C_2–C_4) formation compared to unpromoted Fe catalysts [8–11]. Mo-promoted Fe supported on activated carbon also showed significant catalytic stability [12]. Increased catalytic activity has been observed for FeOOH supported on ZrO_2 [13]. Adding Cr enhanced the selectivity of precipitated Fe catalysts for longer-chain hydrocarbon products [14].

Several research groups have suggested, based on evidence, that Fe carbides, not metallic Fe, play a critical role in the activity of Fe-based catalysts for FTS [15–19]. If this is so, then the active sites of Fe-based FTS catalysts likely should exist in a carburized state on the surface. Therefore, it seems that the ability of the Fe catalyst to maintain a carburized surface may

* Corresponding author. Fax: +1 (864) 656 0784.
E-mail address: james.goodwin@ces.clemson.edu (J.G. Goodwin).

0021-9517/$ – see front matter
doi:10.1016/j.jcat.2008.01.026

be the key to increasing and maintaining its long-term activity. The addition of another transition metal to bulk Fe catalysts could result in improved catalyst activity if it helped maintain or gave rise to the formation of more active carbide species.

Surprisingly, to date there appears to have been little or no study of the impact of a wide variety of different transition metals, such as Cr, Mn, Mo, Ta, V, W, and Zr, on the catalytic properties of bulk Fe-based catalysts having similar preparation methods and reaction conditions. Although the impact of added Mo [12] or Mn [8,10,11,20,21] on the activity of Fe catalysts has been studied, to the best of our knowledge, no study has been done on an Fe-based catalyst containing Cu and SiO_2 similar to a commercial Ruhrchemie catalyst, a standard in the FTS area. The study of the effect of added Zr on Fe FTS catalysts also has been studied only modestly [22]. Most of these studies focused on catalyst systems in which Zr was used as a support (ZrO_2) [23,24]. In addition, fundamental studies of the impact of the addition of Cr, Ta, V, or W on the activity of Fe-based FTS catalysts have not been reported to date, although some patents have claimed the use of Cr and V as promoters for Fischer–Tropsch synthesis catalysts [14,25].

In this work, transition metals such as Cr, Mn, Mo, Ta, V, W and Zr, which are all known to form metal carbides [2], were added to a series of Fe-based catalysts with the general formulations of 100Fe/5Cu/17Si and 95Fe/5*Me*/5Cu/17Si, where *Me* was the third metal present in addition of Fe and Cu (i.e., Cr, Mo, Mn, Ta, V, W or Zr). Metals able to form carbides were hypothesized to have the potential for interesting interactions with Fe since Fe carbide formation occurs during FTS. The formation of mixed metal carbides could even be possible. To distinguish more clearly the effects of *Me*, K promotion was not used for any of the catalysts here. The catalysts were investigated using CO hydrogenation and various characterization techniques. Catalytic activities and selectivities for hydrocarbon products were compared to those for the benchmark catalyst, 100Fe/5Cu/17Si, without third metal promotion.

2. Experimental

2.1. Catalyst preparation

Catalysts for FTS were prepared according to the general formulations of 100Fe/5Cu/17Si (benchmark catalyst) and 95Fe/5*Me*/5Cu/17Si (third metal-promoted Fe catalysts) where *Me* indicates the third transition metal (Cr, Mn, Mo, Ta, V, W or Zr). Compositions are all given on a relative atom basis.

The catalysts (100Fe/5Cu/17Si and 95Fe/5*Me*/5Cu/17Si) were prepared using a pH precipitation technique [26]. For the 100Fe/5Cu/17Si catalyst, $Fe(NO_3)_3{\cdot}9H_2O$ (∼0.6 M) and $CuN_2O_6{\cdot}3H_2O$ were first dissolved together in 60 ml of H_2O, whereas tetraethylorthosilicate ($Si(OC_2H_5)$, TEOS) was dissolved in 40 ml of propanol. The solutions were mixed together and 100 ml of final solution was obtained. The final solution was then heated to 83 ± 3 °C. Subsequently, aqueous NH_4OH (∼2.7 M) preheated to 83 ± 3 °C was continuously added into the solution containing Fe, Cu, and Si precursors under vigorous stirring until precipitation. The resulting pH after formation of a precipitate was 8–9. The precipitate was aged in a vessel at room temperature for 17 h and then thoroughly washed with 1.3–1.5 l of deionized water to remove excess NH_3 until the pH of the washed H_2O was 7–8. The washed precipitate was dried in an oven for 18–24 h at 110 °C to remove excess water. After drying, the catalyst precursor was calcined in static air at 300 °C for 5 h, then cooled to room temperature over a 2-h period in a muffle furnace. The fresh calcined catalyst was sieved <90 μm before reaction testing and other characterizations.

Similarly, 95Fe/5*Me*/5Cu/17Si catalysts were prepared using the same procedure as the 100Fe/5Cu/17Si catalyst except that $Cr(NO_3)_3$, $Mn(NO_3)_2$, MoO_3, $Ta(OC_2H_5)_5$, $V(C_5H_7O_2)_3$, WCl_6, or $ZrO(NO_3)_2$ (as the precursor for Cr, Mn, Mo, Ta, V, W, or Zr, respectively) was dissolved in either the solution of Fe and Cu (in 60 ml of H_2O) or the solution of $Si(OC_2H_5)_4$ (in 40 ml of propanol), depending on its solubility properties. Then the two solutions were mixed to obtain the final solution of 100 ml which was then heated to 83 ± 3 °C. The following steps were then the same as those for the preparation of the 100Fe/5Cu/17Si catalyst. For the W-promoted Fe catalyst, the catalyst was washed 4 times with hot deionized water (90 °C) after calcination to remove any remaining Cl^- impurity from the precursor [27]. Catalyst nomenclatures used are 100Fe, FeCr, FeMn, FeMo, FeTa, FeV, FeW, and FeZr for the benchmark and Cr-, Mn-, Mo-, Ta-, V-, W- and Zr-promoted Fe catalysts, respectively.

2.2. Catalyst characterization

2.2.1. Physical adsorption

BET surface areas, pore volumes and average pore diameters were determined by N_2 physisorption at 77 K using a Micromeritics ASAP 2020 automated system. A 0.3 g catalyst sample was degassed at 100 °C for 1 h and then heated at 10 °C/min to 300 °C and held for 2 h before analysis.

2.2.2. Catalyst composition

Elemental analysis was performed to determine the elemental composition of the fresh calcined catalysts and the carbon content of the catalysts after reaction using inductively coupled plasma optical emission spectrometry (ICP-OES) and the combustion method, respectively. These analyses were done by Galbraith Laboratories Inc. (Knoxville, TN). Elemental compositions of the prepared Fe catalysts as determined by ICP-OES were found to be the expected values within an error of ±10%.

2.2.3. X-ray diffraction (XRD)

The XRD spectra of the catalysts were collected using a Scintag 2000 X-ray diffractometer with monochromatized CuK_α radiation (40 kV, 40 mA) and a Ge detector with a step scan mode at a scan rate of 0.005° (2θ) per second from 10°–90°.

2.2.4. Scanning electron microscopy (SEM) and energy dispersive X-ray spectroscopy (EDX)

The morphologies of the catalyst samples and the elemental concentrations of the catalyst surfaces, as well as elemental distributions, were studied using SEM and EDX, respectively. SEM and EDX were performed using a Hitachi FESEM-S4800 under the scanning electron (SE) mode. The accelerating voltage was 20 kV with a working distance of 14 mm.

2.2.5. Passivation

Characterization of the catalysts after reaction required proper passivation before exposure to air. This procedure was necessary to prevent rapid oxidation of the catalyst upon exposure to O_2 in the air when being removed from the reactor. Passivation was done by introducing a flow of 40 cc/min of 2% O_2 in He to the catalyst at 35 °C. During passivation, the temperature of the catalyst samples generally increased about 5–7 °C then decreased back to the original temperature. When properly performed, passivation leads to only a few nm of an oxide layer on the surface of the catalyst particles [28].

2.2.6. Temperature-programmed reduction (TPR)

Temperature programmed reduction (TPR) was performed using an Altamira AMI-1 system to determine reducibility of the calcined Fe catalysts. The catalysts (0.1 g) were reduced in a flow of 5% H_2/Ar (30 cc/min) with a ramp rate of 2 °C/min to 800 °C. % Fe reducibility also was determined for the reduction procedure used before reaction by ramping the temperature to 280 °C at 2 °C/min and then holding for 12 h before increasing the temperature to 800 °C. A thermal conductivity detector (TCD) was used to measure H_2 consumption. The detector output was calibrated based upon 100% reducibility of Ag_2O powder, and a H_2O trap was used to remove H_2O produced during the reduction.

2.2.7. CO chemisorption

CO chemisorption was performed using a Micromeritics ASAP 2010 automated system. Before CO chemisorption, 0.1 g of fresh calcined catalyst was evacuated to 10^{-6} mm Hg at 100 °C for 30 min; then, it was reduced under flowing H_2 at 280 °C for 12 h (2 °C/min). The catalyst was evacuated again at 280 °C for 60 min to desorb any H_2. The chemisorption analysis was carried out at 35 °C. An average CO:Fe_s stoichiometry of 1:2 was assumed [29].

2.3. Reaction kinetic measurements

Fischer–Tropsch reaction was carried out in a quartz microreactor (i.d. = 8 mm) with a maximum conversion below 10% to minimize temperature and concentration gradients. A catalyst (0.1 g) was pretreated (reduced) *in situ* at 280 °C under 30 cc/min of H_2 (National Specialty Gases, Zero Grade) for 12 h (the temperature was ramped at 2 °C/min). After pretreatment, the catalyst was flushed with 30 cc/min of He (National Specialty Gases, UHP) for 15 min before reaction. The reaction was carried out at 280 °C and a constant pressure of 1.8 atm. The total flow rate of the reaction mixture was kept constant at 60 cc/min (STP) which consisted of 5 cc/min of 95% CO + 5% Ar (National Specialty Gases) and 10 cc/min of H_2 in a balance of He to produce a H_2:CO ratio of 2:1. The reaction line and sampling valves were maintained at 230 °C with heating tape to avoid condensation of higher hydrocarbon products. The effluent samples were analyzed using a Varian 3700 GC equipped with an AT-Q 30 m × 0.53 mm Heliflex capillary column with a flame ionization detector (FID) for hydrocarbon detection and with a Carbosphere 80/100 $6' \times 1/8'' \times 0.085''$ SS packed column with a thermal conductivity detector (TCD) for CO and CO_2 detection.

The reaction carried out in this study was free from heat or mass transfer limitations. No internal or external mass transfer limitations were detected when particle size of the Fe catalyst (38–140 μm) and total flow rate (60–100 cc/min) were varied, respectively. The apparent activation energies (E_a) of the reaction for Fe catalysts were determined by plotting reaction rate vs $1/T$ (not shown). All E_a values were found to be 93–108 kJ/mol over a temperature range of 260–300 °C, similar to what has been reported in the literature [21,30,31]. All experimental rate measurements were reproducible within a maximum error of ±5%.

3. Results and discussion

3.1. Catalyst characterization

3.1.1. BET measurements

The BET surface areas, pore volumes and pore sizes of the catalysts as prepared are shown in Table 1. *Me*-promoted Fe catalysts showed lower average pore sizes but slightly higher BET surface areas than those of the benchmark catalyst (100Fe), with the exception of W which exhibited the lowest surface area.

3.1.2. XRD

There were no discernible diffraction peaks for any oxide phases of Fe, Cu or *Me* for the fresh calcined catalysts (not shown). This indicates that all catalysts were XRD amorphous having average oxide crystallite sizes <4–5 nm based on the wavelength of CuK_α radiation. In this sense, precipitated SiO_2 must have been well dispersed throughout the catalysts causing

Table 1
BET surface area, pore volume and pore size of the Fe-based catalysts

Catalyst[a]	BET S.A.[b] (m^2/g)	Pore volume[b] (cm^3/g)	Average pore[b] size (A)
100Fe	329	0.34	42
FeCr	351	0.29	33
FeMn	354	0.33	38
FeMo	342	0.27	32
FeTa	341	0.29	34
FeV	338	0.26	30
FeW	295	0.25	34
FeZr	350	0.29	33

[a] All catalysts also contain 5Cu and 17Si.
[b] Max error = ±5%.

the average crystallite sizes of even the major component Fe oxides to be very small.

3.1.3. SEM and EDX

Catalyst granule morphologies for the 100Fe catalyst observed using SEM are shown in Fig. 1. In general, catalyst granules were faceted and irregular shaped with some uneven surfaces. No difference in granule morphologies among the catalysts with different metals was observed (not shown). Although SEM revealed that the diameters of the catalyst granules were in the range of 10–60 μm (Fig. 1), all Fe catalysts were XRD amorphous. This suggests that catalyst granules as observed by SEM must have composed of thousands of very small Fe oxide crystallites bound together. It has been suggested that the presence of SiO_2 increases the surface area of precipitated Fe catalysts by preventing the sintering of Fe_2O_3 crystallites [3] and acting as the binding agent [7]. Therefore, very high BET surface areas of catalysts were obtained.

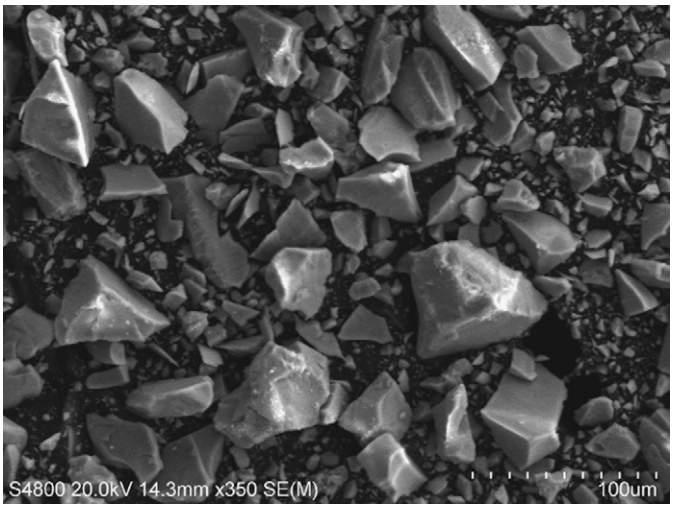

Fig. 1. SEM micrograph of the 100Fe catalyst.

EDX mapping was used to analyze the elemental distribution on the surface of the freshly calcined catalyst particles. As seen in Figs. 2a and 2b for the benchmark 100Fe and FeMn catalysts, respectively, all particles of the catalysts contained primarily ca. 60% Fe (bulk Fe catalysts). All elements also were well distributed on the surface of the catalyst particles, with no obvious segregation. This also was observed for the other *Me*-promoted Fe catalysts (not shown).

3.1.4. Temperature-programmed reduction (TPR)

A comparison of TPR results for all Fe catalysts and a pure Fe_2O_3 powder (reference) is shown in Fig. 3. It is reasonable to assume that only the Fe_2O_3 phase was primarily present after calcination based on the similar TPR profiles for all the Fe catalysts prepared in this study. Previous work in our lab has shown that only Fe_2O_3 is able to be detected after calcination of a similar catalyst system [32]. Comparing the TPR profiles

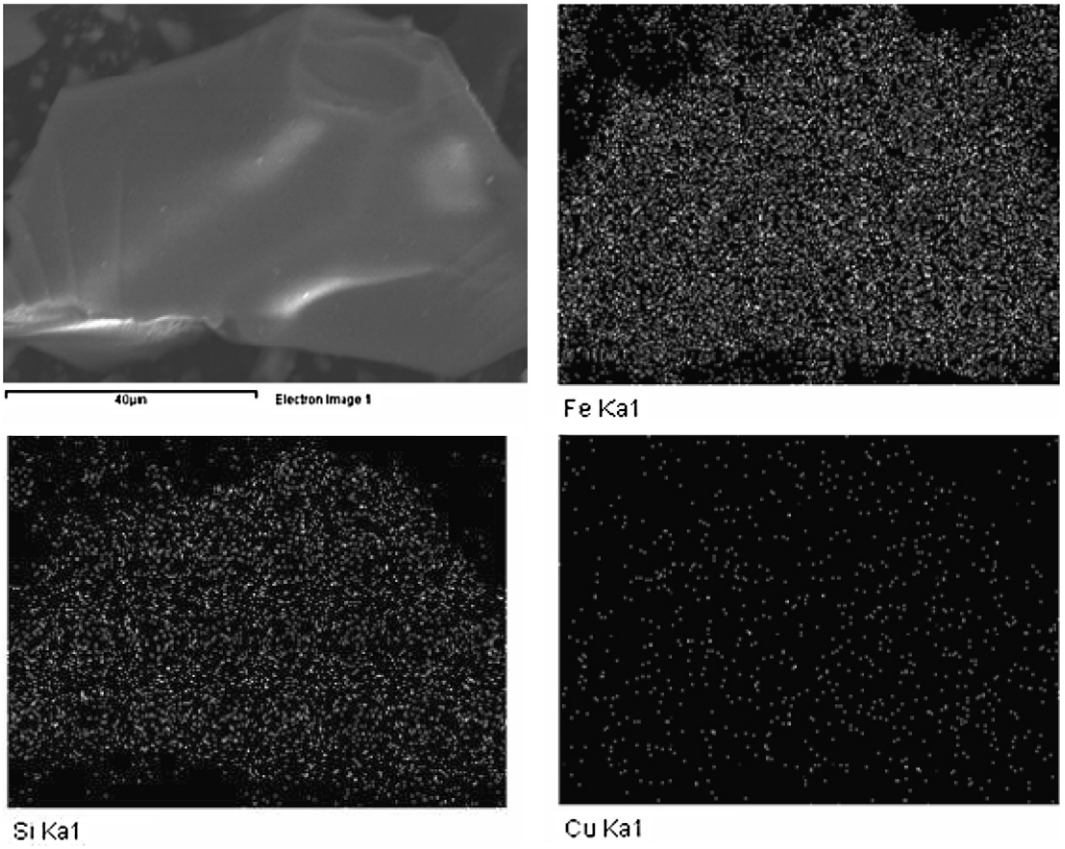

(a)

Fig. 2. SEM micrograph and EDX mapping of fresh calcined (a) 100Fe and (b) FeMn granules.

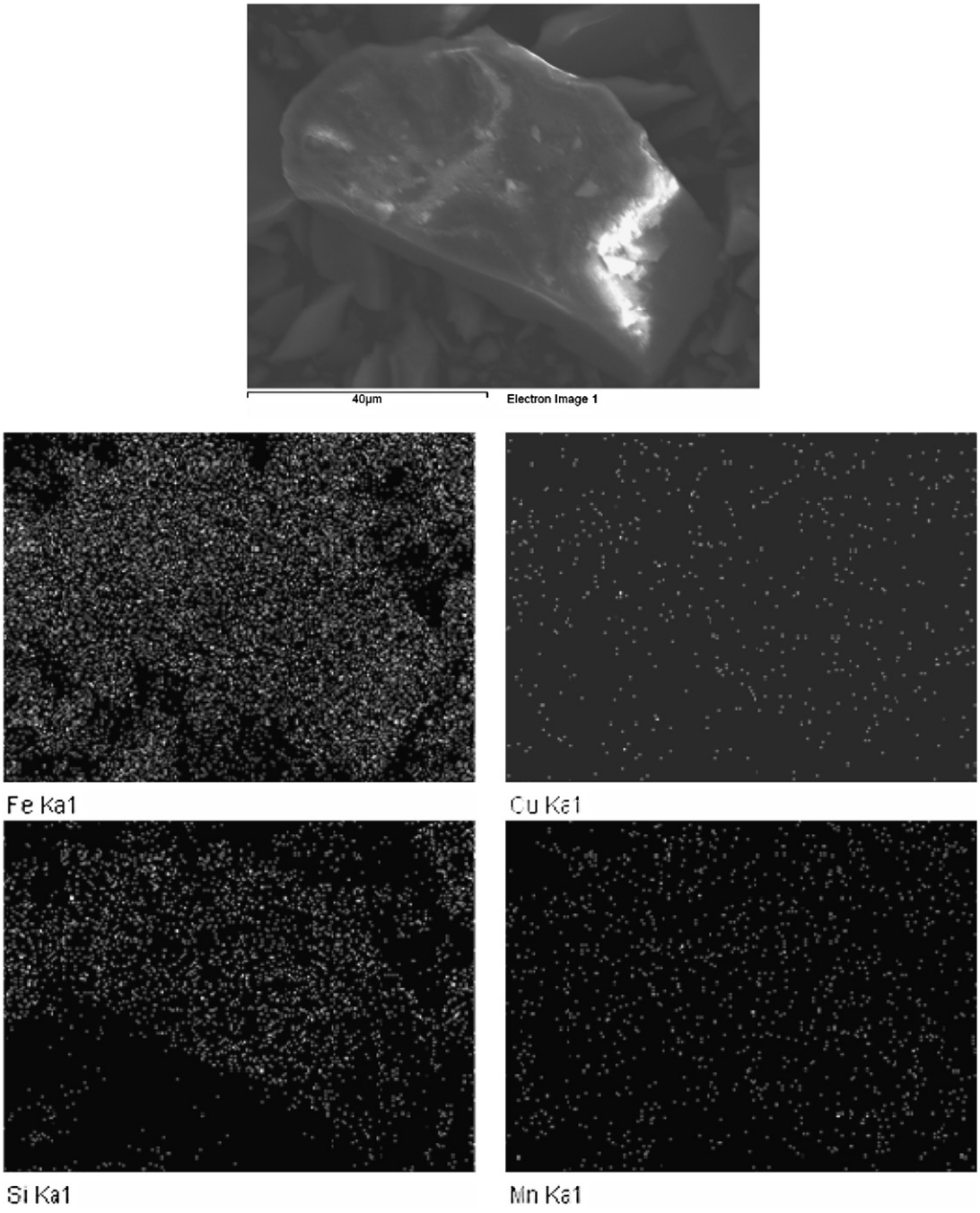

(b)

Fig. 2. (*continued*)

of the calcined Fe-based catalysts and the pure Fe_2O_3 powder clearly shows that the presence of Cu (in all catalysts) facilitated the reducibility of the Fe, as is well known [1,2,5]. Fig. 3 reveals that all the catalysts showed 2 distinct peaks at temperatures of approx. 215 and 600 °C. It has been suggested that the reduction of Fe_2O_3 occurs via 2 main steps: $Fe_2O_3 \rightarrow Fe_3O_4 \rightarrow Fe$. These 2 elementary reactions have been assigned to the first and second peaks in the TPR profiles, respectively [33–35].

To be able to determine the amount of Fe reduced before reaction, the most important reducibility number, TPR was carried out using a similar reduction procedure as used before reaction (i.e., pretreatment in a flow of H_2 at 280 °C for 12 h). After ramping the temperature 2 °C/min to 280 °C, the temperature was held at 280 °C for 12 h before being ramped up to 800 °C. Fig. 4 clearly shows that holding 100Fe at 280 °C for 12 h did not increase the reducibility of Fe. Therefore, only the first reduction peak during TPR accounts for the reduction of Fe under the standard reduction procedure used. % Fe reducibility in Table 2, therefore, was calculated only from the first TPR peaks shown in Fig. 3 and represents the degree of reducibility of the catalysts before chemisorption or reaction. In this complicated catalyst system containing multiple metals, the

Table 2
Results from TPR of and CO-chemisorption on the Fe-based catalysts studied

Catalyst[a]	H_2-TPR		CO-chemisorption	
	Peak temperature[b] (°C)	Fe reducibility[c] (%)	Total CO chemisorbed[d] (μmol/g)	Fe dispersion[e] (%)
100Fe	215	35	120	2.6
FeCr	207	39	232	5.3
FeMn	241	33	155	3.5
FeMo	228	36	148	3.6
FeTa	215	35	139	3.4
FeV	249	36	157	3.8
FeW	222	32	107	2.6
FeZr	215	37	169	3.9

[a] All catalysts also contain 5Cu and 17Si.
[b] Max error = ±2%.
[c] % Fe reduced during standard reduction (280 °C for 12 h). Max error = ±5%.
[d] Determined by extrapolating the total chemisorption isotherm to zero pressure. Max error ±3%.
[e] Based on total CO chemisorbed, % dispersion = 2 × total CO chemisorbed/total number of Fe atoms.

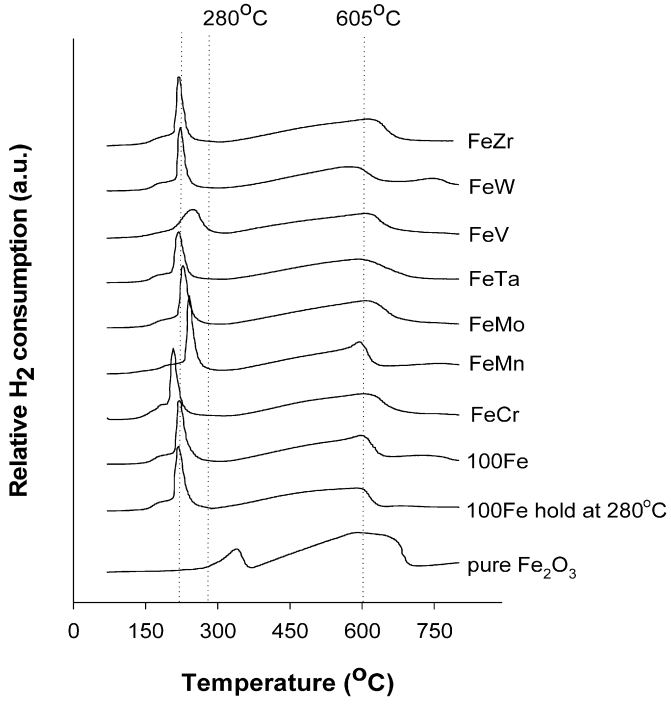

Fig. 3. TPR profiles of the fresh calcined Fe-based catalysts.

calculation of % reducibility of Fe was based on an assumption of only the reduction of $Fe_2O_3 \rightarrow Fe$ since it is likely that some Fe_2O_3 could be reduced to Fe_3O_4 and then Fe rapidly for small Fe crystallites with the presence of Cu. This is not absolutely correct and should only be considered as an approximation.

% Fe reducibility shown in Table 2 reveals that the promotion of Fe catalyst with a third metal did not increase the reducibility of Fe, resulting in relatively the same Fe reducibility of about 32–39%. However, adding a third metal had an impact on the reduction peak temperatures which varied depending upon the added third metal. The reduction peak temperature of FeCr was shifted to a lower temperature at about 207 °C but those for FeMn and FeV were delayed to 241 and 249 °C, respectively. It has been suggested by Lee et al. [36] that MnO can stabilize Fe^{2+}, thus delaying the reduction of Fe^{3+} to Fe^0 to a higher temperature. The higher reduction temperature observed for FeV could have been due to an incorporation of V into the Fe oxide structure as has been suggested by Junior et al. [37]. In contrast, the addition of Mo did not show any impact on the reducibility of Fe, resulting in relatively the same value as the benchmark 100Fe catalyst. Although the study of Ma et al. [12] has shown that Fe supported on activated carbon catalyst was less reduced when Mo was added, this divergence in results may have been due to difference in catalyst compositions or preparation methods.

3.1.5. CO chemisorption

Table 2 also shows total amounts of CO chemisorbed and % Fe dispersion. The amount of chemisorbed CO and % dispersion of 100Fe were 120 μmol/g and 2.6%, respectively. For all third metal-promoted Fe catalysts (except W), these values were in the range of 139–234 μmol/g and 3.4–5.4%, respectively, which were significantly higher than those of 100Fe. FeCr exhibited by far the highest amount of chemisorbed CO and, consequently, the highest % Fe dispersion (i.e., twice that of 100Fe). It is unlikely that this could be significantly affected by chemisorption of CO on Cr since only 19 μmol/g of CO was estimated to chemisorb on Cr [i.e., by extrapolating the total amount of CO chemisorbed on 100Cr/5Cu/17Si with no Fe present and reduced at 280 °C for 12 h to that for a composition of 5Cr (not shown)]. Thus, it would appear that adding a third metal promoted the dispersion of Fe. The only exception was the catalyst containing W where the dispersion of Fe was not improved, showing relatively the same amount of CO chemisorption as the benchmark 100Fe catalyst.

3.2. Catalyst activities

Activities of the prepared Fe-based catalysts for FTS were determined at 280 °C and a H_2/CO ratio of 2:1 and are shown in Figs. 5 and 6 for CO hydrogenation and the WGS reaction, respectively. The catalysts were reduced in H_2 before the reaction as H_2-pretreated Fe catalysts have been shown to give the high-

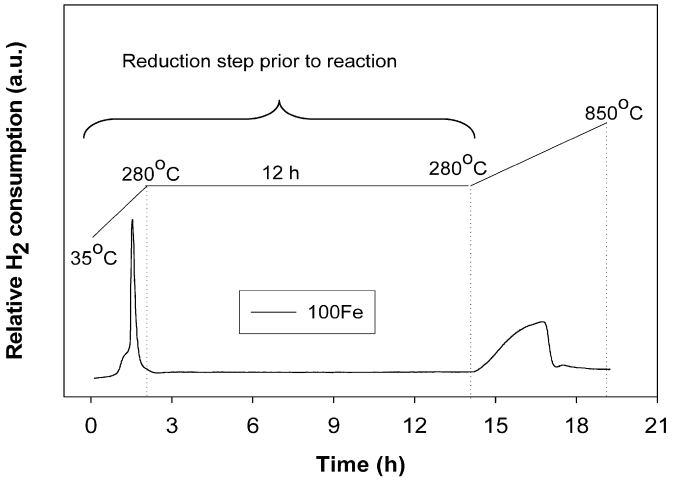

Fig. 4. The TPR profile of 100Fe with a 12 h hold at 280 °C.

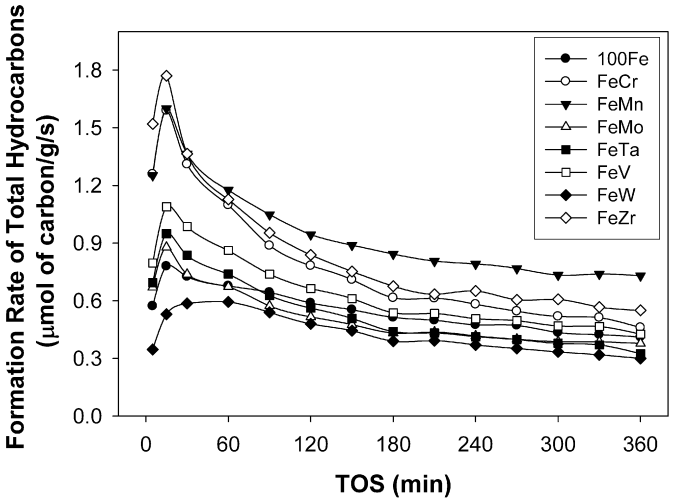

Fig. 5. Formation rates of hydrocarbons (C_1–C_8) at 280 °C with the addition of various transition metals.

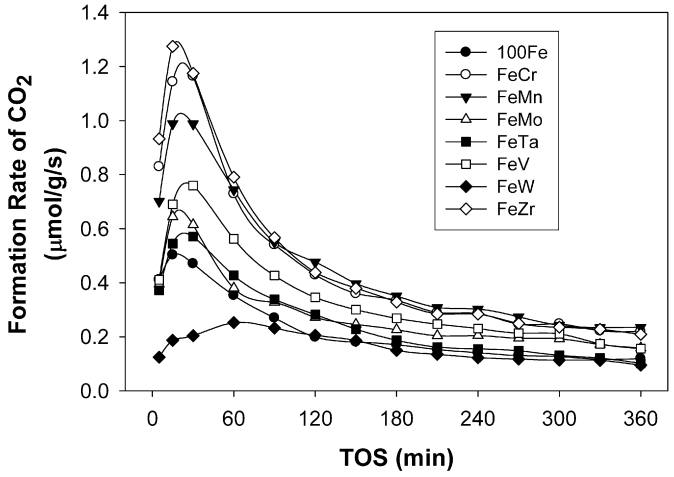

Fig. 6. Formation rates of CO_2 at 280 °C with the addition of various transition metals.

est CO conversion rate [32]. Due to detectability limitations, we were unable to follow hydrocarbon products larger than C_8 since the operational reaction conversion was maintained below 10%.

Interestingly, induction periods were observed for both reactions (CO hydrogenation and WGS reaction) catalyzed by the Fe catalysts. During this period, the activity of catalysts increased to a maximum before declining due to deactivation to a pseudo-steady-state level. Fig. 5 shows that the lengths of the induction periods for CO hydrogenation on all Fe catalysts were identical (ca. 15 min) but varied from 15–30 min for the WGS reaction (Fig. 6). This divergence between induction periods for the two reactions also supports the postulation that different sites are actually involved in their respective catalysis. Van der Laan and Beenackers [38] proposed that Fe carbides are the active phase for hydrocarbon formation whereas Fe_3O_4 is involved in WGS reaction.

It has been suggested that an increase in the activity of a precipitated bulk Fe FTS catalyst during the induction period is due to an increase in the conversion of α-Fe to Fe carbides [18]. From this standpoint, the addition of a third transition metal may have assisted the carburization rate of Fe leading to a higher hydrocarbon formation rate and α during the early stages of reaction. The existence of the reaction induction period for a similar 100Fe/5Cu/4.2K/11SiO_2 catalyst pretreated under H_2 has also been reported by Sudsakorn et al. [32]. Their results, based on steady state isotopic transient kinetic analysis (SSITKA), showed that an increase in the number of active surface intermediates caused the existence of the induction period.

The addition of the third transition metal to the Fe-based catalyst improved FTS catalyst activities for both CO hydrogenation (Fig. 5) and WGS reaction (Fig. 6) in different degrees, depending on the third metal added. Overall, the catalyst activities were in the order FeMn > FeZr > FeCr > FeV > FeTa > FeMo > 100Fe > FeW. Activity improvement was not observed for the addition of W. This was not due to Cl^- poisoning (from the precursor used, WCl_6), because a FeW catalyst prepared using a non-Cl-containing precursor, $(NH_4)_2WO_4$, gave similar activity results (not shown). Therefore, the low activity of the FeW catalyst was likely a combination of its lower surface area and lower Fe dispersion.

The addition of Cr, Mn and Zr enhanced the catalyst activities for CO hydrogenation and the WGS reaction the most. At maximum catalyst activity, the formation rates of total hydrocarbons and CO_2 were about 2–3 times higher than those of the benchmark catalyst (100Fe). The activity of FeMn for CO hydrogenation was very stable and remained higher than that of FeCr and FeZr. It has been suggested that adding Mn to Fe-based catalysts increases the carburization of Fe [11] and the stabilization of the surface active carbonaceous species [21] which could have partly been a cause of the high activity and stability observed for Mn-promoted Fe catalysts. In addition, the addition of Cr and Zr appear to promote the WGS activity of Fe catalyst the most (Fig. 6). Fe_2O_3/Cr_2O_3 catalysts have been well known to carry out WGS reaction [39] while the ability of ZrO_2 to decompose H_2O into active H and O species that could translate into a slightly greater surface concentration of H on this catalyst might in part explain the enhancement in the WGS activity of FeZr observed [13].

Table 3
Activities and selectivities for the Fe-based catalysts.

Catalyst[a]	Maximum rate[b] (μmol of carbon/g/s)		SS rate[b,c] (μmol of carbon/g/s)		Maximum TOF_{chem}[d] $(s^{-1}) \times 10^2$	% hydrocarbon selectivity at SS[b,c,e,f]					% olefin at SS $(C_2–C_4)$[b,c]
	CO_2	Total HC	CO_2	Total HC		C_1	C_2	C_3	C_4	$C_5–C_8$	
100Fe	0.50	0.78	0.13	0.43	0.55	27	29	23	16	5	74
FeCr	1.14	1.59	0.25	0.52	0.59	29	26	25	13	7	75
FeMn	0.99	1.58	0.24	0.72	0.83	29	26	22	18	6	82
FeMo	0.64	0.88	0.19	0.39	0.51	28	27	25	14	6	72
FeTa	0.61	0.95	0.12	0.38	0.56	28	27	25	14	6	74
FeV	0.76	1.09	0.21	0.47	0.59	29	27	25	13	6	72
FeW	0.25	0.53	0.11	0.33	0.37	29	28	26	13	4	68
FeZr	1.27	1.77	0.24	0.61	0.90	28	26	23	21	2	81

[a] All catalysts also contain 5Cu and 17Si.
[b] Max error = ±5%.
[c] At 300 min TOS.
[d] Calculated from TOF_{chem} = reaction rate (at the maximum activity)/amount CO chemisorbed. Max error = ±10%.
[e] Based on atomic carbon.
[f] Any oxygenate compounds produced during reaction in this study were below the detectability limit of the FID detector used.

A summary of reaction rates, TOF_{chem}s, %hydrocarbon selectivities, and % $C_2–C_4$ olefin selectivities for the *Me*-promoted and the benchmark Fe catalysts are reported in Table 3. The activities of the catalysts at their maxima were used to calculate TOF_{chem}s. Although the results from CO chemisorption in Table 2 showed that % Fe dispersion of FeMn and FeZr was significantly lower than that of FeCr, the activities of these 2 catalysts were indistinguishable from those of FeCr (Figs. 5 and 6). The results in Table 3 suggest that the higher activities observed for the FeMn and FeZr catalysts were possibly due to higher TOF_{chem} values (0.008–0.009 s^{-1}). On the contrary, based on the CO chemisorption and TOF results (Tables 2 and 3), the greater overall activity observed for FeCr, FeMo, FeTa, and FeV may have been due simply to the presence of a greater number of Fe sites.

Table 3 also reveals that the %selectivity for hydrocarbons was not greatly affected by the presence of the third metal, showing relatively the same values as those of 100Fe. % Selectivity for CH_4, C_3 (propylene and propane) and C_4 (*n*-butane, butene, and isobutane) hydrocarbons remained unchanged with TOS, while % $C_2–C_4$ olefins (ethylene, propylene and butene) increased with TOS for all catalysts (not shown). The changes in % selectivity of low-molecular-weight hydrocarbons, C_2 (ethane), $C_2^=$ (ethylene), C_3 (propane) and $C_3^=$ (propylene), with TOS for the benchmark 100Fe, FeCr, FeMn, and FeZr are shown in Fig. 7. % Selectivity for propylene gradually increased, but the selectivity for ethylene increased even more significantly. On the other hand, ethane and propane selectivities slightly decreased with TOS. The increase in propylene selectivity was balanced by the decrease in propane selectivity, thus giving rise to a constant selectivity for C_3 (propylene and propane) hydrocarbons. This trend was observed for all catalysts studied here; (the results for only the 3 most active catalysts and the benchmark 100Fe catalyst are shown in Fig. 7 to make the figure easier to read).

Changes in the chain growth probability (α) with TOS of various Fe FTS catalysts are plotted in Fig. 8. The chain growth probability was initially higher with third metal promotion (except for W) compared to the benchmark catalyst (100Fe). However, after 5 h TOS, all catalysts exhibited similar values of α equivalent to that initially observed for 100Fe which was about 0.35. An accurate measure of the chain growth probability of FeW could not be obtained due to its low activity; thus, Fig. 8 does not include the α values for FeW. It has been shown that a decrease in the number of potential Fe sites is the cause of catalyst deactivation as determined by SSITKA (steady state isotopic transient kinetic analysis) [32]. As the catalyst deactivated, there were less sites available for ethylene to readsorb on and participate in chain growth [40,41]. Thus, the increase in the formation of ethylene could have resulted as a consequence of the decrease in α at long TOS.

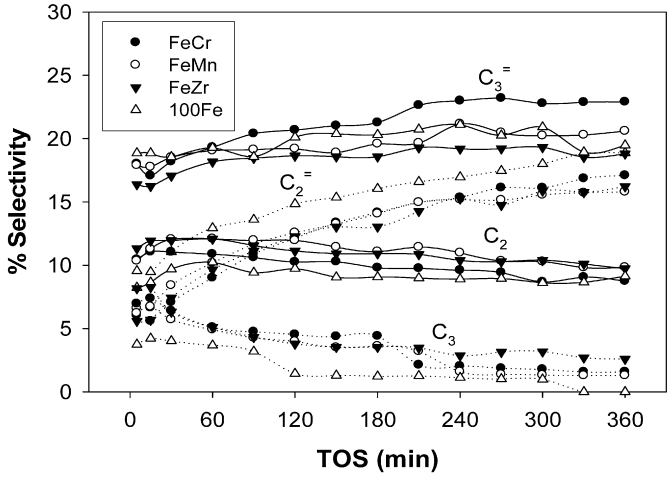

Fig. 7. The % selectivities for $C_2^=$, C_2, $C_3^=$ and C_3 at 280 °C for the FeCr, FeMn, and FeZr catalysts.

The amount of carbon deposition on the surface of the benchmark catalyst (100Fe) as a function of TOS was determined and is shown in Fig. 9. During the first 2 h of reaction, significant amounts of carbon loss from the product stream were determined by mass balance analysis. The amount of carbon consumed (CO conversion) was found to be greater than that of the total carbon in the gaseous products detected (CO_2

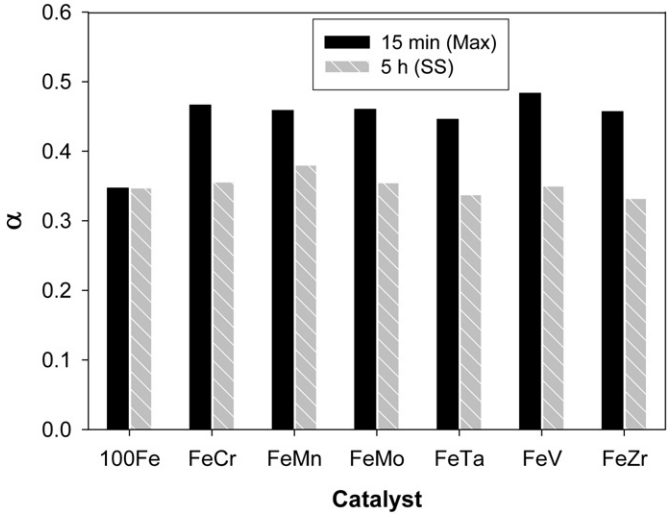

Fig. 8. Calculated chain growth probabilities (α) with TOS for the various Fe-based catalysts.

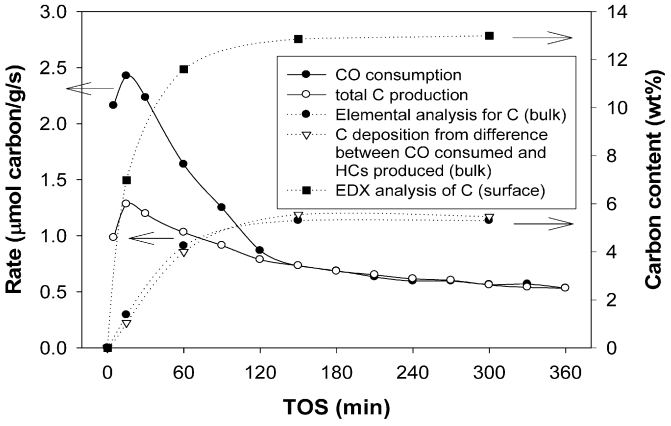

Fig. 9. A comparison of CO consumption, total carbon production, and the catalyst carbon content with TOS for the 100Fe catalyst.

and hydrocarbon products), as shown in Fig. 9. This also was observed for the other *Me*-promoted Fe catalysts (not shown). Therefore, by determining the area between the carbon consumption (CO) and total carbon production (CO_2 + total hydrocarbons) curves in Fig. 9, the amount of carbon deposited on 100Fe was obtained and plotted as a function of TOS (Fig. 9). These values are essentially identical with those obtained using carbon elemental analysis. Thus, it can be concluded that the loss in carbon from the product stream was due to the irreversible deposition of carbon on the surface of the catalyst, some of which must have been involved in the formation of Fe carbides, as suggested to be active reaction phases for FTS [15,16,18].

Significant amounts of deposited carbon on the catalyst surface were also observed using EDX. This surface carbon concentration was found to be 2 times greater than the bulk carbon concentration obtained from elemental analysis and curve integration (Fig. 9). The carbon determined by EDX can be considered as carbon on or within a few nm of the surface. Carbon deposition determined by elemental analysis and curve integration of reaction data represents carbon deposition for the whole catalyst (bulk concentrations). EDX results clearly show that large amounts of carbon remained on the catalyst surface after the first hour of reaction and were significantly higher than that in the bulk. Based on the results shown in Fig. 9, carburization of metallic Fe takes place most probably during the first 1–2 h of reaction, as also reported by Niemantsverdriet et al. [18].

4. Conclusions

The addition of a third transition metal (Cr, Mo, Mn, Ta, V or Zr) to FeCu-based FTS catalysts increased the catalyst activity for both CO hydrogenation and WGS activity in varying degrees. The addition of W, however, led to lower activity. The dispersion of Fe was enhanced by the addition of all metals studied with the exception of W. Cr, Mn and Zr appear to be the best able to enhance the activity of Fe-based catalysts. WGS activities of these 3 catalysts (FeCr, FeMn, and FeZr) were shown to be superior; therefore, they should be able to catalyze FTS under lower H_2/CO ratio syngas derived from biomass or coal.

The high activity observed for the Fe-based catalyst with Cr, Mo, Ta, and V addition was likely due to better Fe dispersions. The high catalytic activities for Mn- and Zr-promoted Fe catalysts, on the other hand, may have been due more to higher intrinsic site activities, as estimated by TOF_{chem} based on CO chemisorption. The selectivities for hydrocarbons and the chain growth probability (α) were not significantly affected, especially at pseudo-steady state, by the addition of any third transition metal.

Acknowledgments

This paper is based upon work supported by National Association of State Energy Offices (NASEO) grant No. DE-FC36-03G013026. Any opinions, findings, and conclusions or recommendations expressed in this paper are those of the authors and do not necessarily reflect the views of the NASEO.

References

[1] H.H. Storch, N. Golumbic, R.B. Anderson, The Fischer–Tropsch and Related Synthesis, Wiley, New York, 1951.
[2] R.B. Anderson, The Fischer–Tropsch Synthesis, Academic Press, Orlando, FL, 1984.
[3] M.E. Dry, The Fischer–Tropsch synthesis, in: J.R. Anderson, M.E. Boudart (Eds.), Catalysis—Science and Technology, Springer-Verlag, New York, 1981, pp. 159–255.
[4] Y.M. Jin, A.K. Datye, J. Catal. 196 (2000) 8–17.
[5] S.Z. Li, S. Krishnamoorthy, A.W. Li, G.D. Meitzner, E. Iglesia, J. Catal. 206 (2002) 202–217.
[6] R.J. O'Brien, L.G. Xu, R.L. Spicer, S.Q. Bao, D.R. Milburn, B.H. Davis, Catal. Today 36 (1997) 325–334.
[7] K. Sudsakorn, J.G. Goodwin Jr., K. Jothimurugesan, A.A. Adeyiga, Ind. Eng. Chem. Res. 40 (2001) 4778–4784.
[8] L. Bai, H.W. Xiang, Y.W. Li, Y.Z. Han, B. Zhong, Fuel 81 (2002) 1577–1581.
[9] R. Malessa, M. Baerns, Ind. Eng. Chem. Res. 27 (1988) 279–283.
[10] C. Wang, Q.X. Wang, X.D. Sun, L.Y. Xu, Catal. Lett. 105 (2005) 93–101.
[11] T.Z. Li, Y. Yang, C.H. Zhang, X. An, H.J. Wan, Z.C. Tao, H.W. Xiang, Y.W. Li, F. Yi, B.F. Xu, Fuel 86 (2007) 921–928.

[12] W. Ma, E.L. Kugler, J. Wright, D.B. Dadyburjor, Energy Fuel 20 (2006) 2299–2307.
[13] T. Masuda, Y. Kondo, M. Miwa, T. Shimotori, S.R. Mukai, K. Hashimoto, M. Takano, S. Kawasaki, S. Yoshida, Chem. Eng. Sci. 56 (2001) 897–904.
[14] T.C. Bromfield, R. Visagie, Chromium oxide incorporation into precipitated iron-based Fischer–Tropsch catalysts for increased production of oxygenates and branched hydrocarbons, patent # WO2005/049765A1, 2005, USA.
[15] S.Z. Li, R.J. O'Brien, G.D. Meitzner, H. Hamdeh, B.H. Davis, E. Iglesia, Appl. Catal. A 219 (2001) 215–222.
[16] G. LeCaer, J.M. Dubois, M. Pijolat, V. Perrichon, P. Bussiere, J. Phys. Chem. 86 (1982) 4799–4808.
[17] M.D. Shroff, D.S. Kalakkad, K.E. Coulter, S.D. Kohler, M.S. Harrington, N.B. Jackson, A.G. Sault, A.K. Datye, J. Catal. 156 (1995) 185–207.
[18] J.W. Niemantsverdriet, A.M. van der Kraan, W.L. van Dijk, H.S. van der Baan, J. Phys. Chem. 84 (1980) 3363–3370.
[19] W.S. Ning, N. Koizumi, H. Chang, T. Mochizuki, T. Itoh, M. Yamada, Appl. Catal. A 312 (2006) 35–44.
[20] Y. Yang, H.W. Xiang, Y.Y. Xu, L. Bai, Y.W. Li, Appl. Catal. A 266 (2004) 181–194.
[21] T. Herranz, S. Rojas, F.J. Perez-Alonso, M. Ojeda, P. Terreros, J.L.G. Fierro, J. Catal. 243 (2006) 199–211.
[22] R.J. Obrien, L.G. Xu, D.R. Milburn, Y.X. Li, K.J. Klabunde, B.H. Davis, Top. Catal. 2 (1995) 1–15.
[23] K.D. Chen, Y.N. Fan, Z. Hu, Q.J. Yan, Catal. Lett. 36 (1996) 139–144.
[24] K.D. Chen, Y.N. Fan, Q.J. Yan, J. Catal. 167 (1997) 573–575.
[25] R.D. Cortright, and J.A. Dumesic, Method for producing bio-fuel that integrates heat from carbon–carbon bond-forming reactions to drive biomass gasification reactions, application # 20070225383, 2007, USA.
[26] D.B. Bukur, X.S. Lang, J.A. Rossin, W.H. Zimmerman, M.P. Rosynek, E.B. Yeh, C.P. Li, Ind. Eng. Chem. Res. 28 (1989) 1130–1140.
[27] G. Beeston, Treatment of residues, patent # 1250913, 1971, England.
[28] M.D. Shroff, A.K. Datye, Catal. Lett. 37 (1996) 101–106.
[29] H.J. Jung, M.A. Vannice, L.N. Mulay, R.M. Stanfield, W.N. Delgass, J. Catal. 76 (1982) 208–224.
[30] G.P. Van der Laan, A.A.C.M. Beenackers, Catal. Rev. 41 (1999) 255–318.
[31] S.A. Eliason, C.H. Bartholomew, Appl. Catal. A 186 (1999) 229–243.
[32] K. Sudsakorn, J.G. Goodwin Jr., A.A. Adeyiga, J. Catal. 213 (2003) 204–210.
[33] D.B. Bukur, C. Sivaraj, Appl. Catal. A 231 (2002) 201–214.
[34] I.S.C. Hughes, J.O.H. Newman, G.C. Bond, Appl. Catal. 30 (1987) 303–311.
[35] K. Jothimurugesan, J.G. Goodwin Jr., S.K. Gangwal, J.J. Spivey, Catal. Today 58 (2000) 335–344.
[36] M.D. Lee, J.F. Lee, C.S. Chang, T.Y. Dong, Appl. Catal. 72 (1991) 267–281.
[37] I.L. Junior, J.M.M. Millet, M. Aouine, M. do Carmo Rangel, Appl. Catal. A 283 (2005) 91–98.
[38] G.P. van der Laan, A.A.C.M. Beenackers, Appl. Catal. A 193 (2000) 39–53.
[39] R.L. Keiski, T. Salmi, Appl. Catal. A 87 (1992) 185–203.
[40] S. Novak, R.J. Madon, H. Suhl, J. Catal. 77 (1982) 141–151.
[41] E. Iglesia, S.C. Reyes, R.J. Madon, J. Catal. 129 (1991) 238–256.